THE LIGHT FRONT ANALYSIS OF π^- MESONS PRODUCED IN THE RELATIVISTIC NUCLEUS-NUCLEUS COLLISIONS

M.Anikina[1], **L.Chkhaidze**[2], **T.Djobava**[2],
V.Garsevanishvili [3,4], **L.Kharkhelauri**[2]

[1] Joint Institute for Nuclear Research, 141980 Dubna, Russia
[2] High Energy Physics Institute, Tbilisi State University,
University Str. 9, 380086 Tbilisi, Republic of Georgia
[3] Mathematical Institute of the Georgian Academy of Sciences
M.Alexidze Str. 1 , 380093 Tbilisi, Republic of Georgia
[4] CERN, CH-1211, Geneva 23, Switzerland

E-mail: djobava@sun20.hepi.edu.ge

ABSTRACT

The light front analysis of π^- mesons in A_P (He, C, Mg, O) + A_T (Li,C, Ne, Mg,Cu,Pb) collisions is carried out. The phase space of secondary pions is naturally divided into two parts in one of which the thermal equilibration assumption seems to be in a good agreement with data. Corresponding temperatures are extracted and compared to the results of other experiments. The dependence of the average temperature T on $(A_P{*}A_T)^{1/2}$ is studied.

PACS. 25.70.-z; Low and intermediate energy heavy-ions reactions

NUCLEAR REACTION The light front analysis of π^- mesons in A_P (He, C, Mg, O) + A_T (Li,C, Ne, Mg,Cu,Pb) collisions is carried out. In some region of phase space of π^- mesons the thermal equilibration seems to be reached, which is characterized by the temperature T.

Keywords: π^- mesons, light front variables, phase space, thermal equilibration.

1. INTRODUCTION

In the experiments with beams of relativistic heavy ions one hopes to observe the extreme conditions when the phase transitions in nuclear matter are expected (see, e.g. [1-3]).

For the experimental study of such transitions it is necessary to understand the mechanism of collisions and investigate the characteristics of multiparticle production in nucleus-nucleus interactions. The study of single particle inclusive processes is one of the simplest and effective tools for the understanding of dynamics of multiple production of secondaries.

In this respect it is important to investigate the properties of π^- mesons, which are predominantly produced particles carrying the information about the dynamics of collision and which are reliably identified. Besides, the pion production is the predominant production process at Dubna energies.

Our previous results on pion production experiment (cross-sections, multiplicities, rapidities, transverse momenta, intercorrelations between various characteristics, etc) using the streamer chamber spectrometer SKM-200 and its modified version GIBS in inelastic and central nucleus-nucleus interactions are presented in [4-6].

In this paper we present the light front analysis of π^- mesons produced in He-Li, He-C, C-Ne, Mg-Mg, C-Cu and O-Pb collisions. In some cases this type of analysis [7] seems to be more sensitive to the details of the interaction mechanism as compared to the presentation of data in terms of the well known variables x_F, rapidity etc.

2. EXPERIMENT

The data were obtained using the SKM-200 facility and its modified version GIBS of the Dubna Joint Institute for Nuclear Research. SKM-200-GIBS consists of a 2m streamer chamber, placed in a magnetic field of $\sim$ 0.8 T and a triggering system. The streamer chamber was exposed by beams of He , C , O , Ne and Mg nuclei accelerated in the synchrophasotron up to a momentum of 4.5 GeV/c per incident nucleon . The solid targets in the form of thin discs with thickness $0.2 \div 0.4$ g/cm^2 (for Li the thickness was 1.59 g/cm^2 and for Mg 1.56 g/cm^2) were mounted within the fiducial volume of the chamber. Neon gas filling of the chamber served also as a nuclear target. The triggering system allowed the selection of "inelastic" and "central" collisions.

The inelastic trigger selected all inelastic interactions of the incident nuclei on the target. The central trigger selected events with no charged projectile spectator fragments (with $P/Z > 3$ GeV/c) within a cone of half angle $\Theta_{ch} = 2.4^0$ or 2.9^0 (the trigger efficiency was 99% for events with a single charged particle in the cone). Later a neutron detector was added to the veto system for excluding events with spectator neutrons in a cone of half angle $\Theta_n = 1.8^0$ or 2.8^0(the trigger efficiency was 80% for events with a single neutron in the cone). The trigger mode for each exposure is defined as T (Θ_{ch} ,Θ_n) (Θ_{ch} and Θ_n expressed in degrees and rounded to the closest integer value). Thus T(0,0) corresponds to all inelastic collisions. For He-Li and He-C collisions we had only an inelastic trigger. The experimental setup and the logic of the triggering systems are presented in Fig.1.

Primary results of scanning and measurements were biased due to several experimental effects and appropriate corrections were introduced. The biases and correction procedures were discussed in detail in [4,5]. Average measurement errors of the momentum and production angle determination for π^- mesons are $< \Delta P/P >= 5\%$, $\Delta\Theta = 0.5^0$ for He-Li, He-C, C-Ne, C-Cu, O-Pb and $< \Delta P/P >= 1.5\%$, $\Delta\Theta = 0.1^0$ for Mg-Mg.

3. LIGHT FRONT PRESENTATION OF INCLUSIVE DISTRIBUTIONS

The study of single particle inclusive processes [8] remains one of the simplest and effective tools for the investigation of multiple production of secondaries at high energies. An important role in establishing of many properties of multiple production is played by the choice of kinematical variables in terms of which observable quantities are presented (see in this connection, e.g. [9]). The variables which are commonly used are the following: the Feynman $x_F = 2p_z/\sqrt{s}$, rapidity $y = \frac{1}{2}\ln[(E+p_z)/(E-p_z)]$, transverse scaling variable $x_T = 2p_T/\sqrt{s}$ etc. In the case of azimuthal symmetry the surfaces of const x_F are the planes $p_z = x_F\sqrt{s}/2$, surfaces of constant y are the hyperboloids

$$p_z^2\left[\left(\frac{1+e^{2y}}{1-e^{2y}}\right)^2 - 1\right] - p_T^2 = m^2$$

and the surfaces of constant x_T are the straight lines $p_T = x_T\sqrt{s}/2$ in the phase space.

Here we propose unified scale invariant variables for the presentation of single particle inclusive distributions, the properties of which are described below.

Consider an arbitrary 4–momentum $p_\mu(p_0, \vec{p})$ and introduce the light front combinations [10]:

$$p_\pm = p_0 \pm p_3 \tag{1}$$

If the 4–momentum p_μ is on the mass shell ($p^2 = m^2$), the combinations $p_\pm,\ \vec{p}_T$ (where $\vec{p}_T = (p_1,\ p_2)$) define the so called horospherical coordinate system (see, e.g. [11]) on the corresponding mass shell hyperboloid $p_0^2 - \vec{p}^{\,2} = m^2$.

Let us construct the scale invariant variables [7]:

$$\xi^\pm = \pm \frac{p_\pm^c}{p_\pm^a + p_\pm^b} \tag{2}$$

in terms of the 4–momenta $p_\mu^a,\ p_\mu^b,\ p_\mu^c$ of particles $a,\ b,\ c$, entering the inclusive reaction $a + b \to c + X$. The z-axis is taken to be the collision axis, i.e. $p_z = p_3 = p_L$. Particles a and b can be hadrons, heavy ions, leptons. The light front variables $\xi^\pm$ in the centre of mass frame are defined as follows [7]:

$$\xi^\pm \ = \ \pm \frac{E \pm p_z}{\sqrt{s}} = \pm \frac{E + |p_z|}{\sqrt{s}} \tag{3}$$

where s is the usual Mandelstam variable, $E = \sqrt{p_z^2 + p_T^2 + m^2}$ and p_z are the energy and the z - component of the momentum of produced particle. The upper sign in Eq. (3) is used for the right hand side hemisphere and the lower sign for the left hand side hemisphere. It is convenient also to introduce the variables

$$\zeta^\pm = \mp \ln|\xi^\pm|$$

in order to enlarge the scale in the region of small $\xi^\pm$.

The invariant differential cross section in terms of these variables looks as follows:

$$E\frac{d\sigma}{d\vec{p}} = \frac{|\xi^\pm|}{\pi}\ \frac{d\sigma}{d\xi^\pm dp_T^2} = \frac{1}{\pi}\ \frac{d\sigma}{d\zeta^\pm dp_T^2} \tag{4}$$

Consider two limiting cases:

1) $|p_z| \gg p_T$ - fragmentation region, according to the common terminology.
In this case:

$$\xi^\pm \to \frac{2p_z}{\sqrt{s}} = x_F \tag{5}$$

2) $p_T \gg |p_z|$ - high p_T-region.
In this case:

$$\xi^\pm \to \frac{m_T}{\sqrt{s}} \to \frac{p_T}{\sqrt{s}} = \frac{x_T}{2}\ ;\ m_T = \sqrt{p_T^2 + m^2} \tag{6}$$

Thus, in these two limiting regions of $\xi^\pm$–variables go over to the well known variables x_F and x_T, which are intensively used in high energy physics.

$\xi^{\pm}$–variables are related to x_F, x_T and rapidity y as follows:

$$\xi^{\pm} = \frac{1}{2}\left(x_F \pm \sqrt{x_F^2 + x_T^2}\right) \; ; \; x_T = \frac{2m_T}{\sqrt{s}} \tag{7}$$

$$y = \pm\frac{1}{2}\ln\frac{(\xi^{\pm}\sqrt{s})^2}{m_T^2} \tag{8}$$

The principal differences of $\xi^{\pm}$ distributions as compared to the corresponding x_F – distributions are the following: 1) existence of some forbidden region around the point $\xi^{\pm} = 0$, 2) existence of maxima at some $\tilde{\xi^{\pm}}$ in the region of relatively small $|\xi^{\pm}|$, 3) existence of the limits for $|\xi^{\pm}| \leq m/\sqrt{s}$. The maximum at $\tilde{\zeta^{\pm}}$ is also observed in the invariant differential cross section $\frac{1}{\pi}\frac{d\sigma}{d\zeta^{\pm}}$. However, the region $|\xi^{\pm}| > |\tilde{\xi^{\pm}}|$ goes over to the region $|\zeta^{\pm}| < |\tilde{\zeta^{\pm}}|$ and vice versa.

Note that the light front variables have been introduced long time ago by Dirac [10] and they are widely used now in the treatment of many theoretical problems (see, e.g. original and review papers [11-20] and references therein). They have been used also in a number of phenomenological applications (see, e.g. [21]).

4. THE ANALYSIS OF PION DISTRIBUTIONS IN TERMS OF LIGHT FRONT VARIABLES

The analysis has been carried out for the π^- mesons from He(Li,C), C-Ne, Mg-Mg, C-Cu and O-Pb collisions. In Figs.2,3 the x_F – and $\xi^{\pm}$ – distributions of π^- mesons from He(Li,C), C-Cu and O-Pb interactions are presented. These distributions are similar for all analysed pairs of nuclei. The experimental data for invariant distributions $(1/\pi) \cdot dN/d\zeta^{\pm}$ in He(Li,C), C-Cu and O-Pb collisions are shown in Fig.4. The curves are the result of the polynomial approximation of the experimental distributions and the maxima are observed in these distributions at $\zeta^{\pm} = \tilde{\zeta^{\pm}}$ ($\tilde{\zeta^{\pm}} = 2.0 \pm 0.3$ for He(Li,C), Mg-Mg, C-Cu and O-Pb; $\tilde{\zeta^{\pm}} = 2.1 \pm 0.3$ for C-Ne). The values of $\tilde{\zeta^{\pm}}$ are the boundaries of the two regions with significantly different characteristics of secondaries.

In Figs.5(a,b,c), 6(a,b,c) the p_T^2 and the angular distributions of π^- mesons from He(Li,C), Mg-Mg, C-Cu and O-Pb interactions in different regions of ζ^+ ($\zeta^+ > \tilde{\zeta^+}$ and

$\zeta^+ < \tilde{\zeta^+}$) in the forward hemisphere are presented. Similar results have been obtained for the backward emitting π^- mesons and for all analysed pairs of nuclei.

One can see from Figs.5,6, that the p_T^2 and the angular distributions of π^- mesons differ significantly in $\zeta^+ > \tilde{\zeta^+}$ and $\zeta^+ < \tilde{\zeta^+}$ regions. The angular distribution of pions in the region $\zeta^+ < \tilde{\zeta^+}$ (Figs.6.a and 6.c) is sharply anisotropic in contrast to the almost flat distribution in the region $\zeta^+ > \tilde{\zeta^+}$ (Figs.6.a and 6.b). The slopes of p_T^2 – distributions differ greatly in different regions of $\zeta^\pm$ (Fig.5.a, 5.b, 5.c). The average values $< p_T^2 >$ in these two regions also differ (e.g. for π^- mesons from Mg-Mg: $< p_T^2 >= (0.027 \pm 0.002)$ $(\mathrm{GeV/c})^2$ in the region $\zeta^+ > \tilde{\zeta^+}$; $< p_T^2 >= (0.103 \pm 0.009)$ $(\mathrm{GeV/c})^2$ in the region $\zeta^+ < \tilde{\zeta^+}$).

The flat behaviour of the angular distribution allows one to think that one observes a partial thermal equilibration in the region $|\zeta^\pm| > |\tilde{\zeta^\pm}|$ ($|\xi^\pm| < |\tilde{\xi^\pm}|$) of phase space.

Note, that the surfaces of constant ξ^+ are the paraboloids

$$p_z = \frac{p_T^2 + m^2 - (\xi^+\sqrt{s})^2}{-2\xi^+\sqrt{s}} \tag{9}$$

in the phase space. Thus the paraboloid

$$p_z = \frac{p_T^2 + m^2 - (\tilde{\xi}^+\sqrt{s})^2}{-2\tilde{\xi}^+\sqrt{s}} \tag{10}$$

separates two groups of particles with significantly different characteristics.

To describe the spectra in the region $\zeta^+ > \tilde{\zeta^+}$ the Boltzmann

$$f(E) \sim e^{-E/T}$$

and the Bose-Einstein (B-E)

$$f(E) \sim (e^{-E/T} - 1)^{-1}$$

distributions have been used.

The distributions $1/\pi \cdot dN/d\zeta^+$, dN/dp_T^2, $dN/dcos\Theta$ look in this region as follows :

$$\frac{1}{\pi}\,\frac{dN}{d\zeta^+} \;\sim\; \int_0^{p_{T,max}^2} E f(E) dp_T^2 \tag{11}$$

$$\frac{dN}{dp_T^2} \;\sim\; \int_0^{p_{z,max}} f(E) dp_z \tag{12}$$

$$\frac{dN}{d\cos\theta} \;\sim\; \int_0^{p_{max}} f(E) p^2 dp \tag{13}$$

$$E \;=\; \sqrt{\vec{p}^{\,2} + m_\pi^2}\ ,\ \vec{p}^{\,2} = p_z^2 + p_T^2 \tag{14}$$

where:

$$p^2_{T,max} = (\tilde{\xi^+}\sqrt{s})^2 - m^2_\pi$$

$$p_{z,max} = [p^2_T + m^2 - (\tilde{\xi^+}\sqrt{s})^2]/(-2\tilde{\xi^+}\sqrt{s})$$

$$p_{max} = (-\tilde{\xi^+}\sqrt{s}cos\Theta + \sqrt{(\tilde{\xi^+}\sqrt{s})^2 - m^2_\pi sin^2\Theta})/sin^2\Theta$$

The experimental distributions in the region $\zeta^+ > \tilde{\zeta^+}$ have been fitted by the expressions (11), (12), (13), respectively. The results of the fit are given in Table 1 and Figs. 5-7. They show a rather good agreement with experiment.

In the region $\zeta^+ < \tilde{\zeta^+}$ the p^2_T – distributions has been fitted by the formula

$$\frac{dN}{dp^2_T} \sim \alpha \cdot e^{-\beta_1 P^2_T} + (1-\alpha) \cdot e^{-\beta_2 p^2_T} \tag{15}$$

and the ζ^+ – distributions by the formula

$$\frac{1}{\pi} \cdot \frac{dN}{d\zeta^+} \sim (1-\xi^+)^n = (1 - e^{-|\zeta^+|})^n \tag{16}$$

The results of the fit are given in Table 2 and Figs.5 and 7.

Thus the spectra of π^- mesons in the region $\zeta^+ > \tilde{\zeta^+}$ are satisfactorily described by the formulae which follow from the thermal equilibration. The same formulae when extrapolated to the region $\zeta^+ < \tilde{\zeta^+}$ (Fig.7.a for Mg-Mg and 7.b for C-Cu) deviate significantly from the data. On the other hand the dependence $(1-\xi^+)^n$ is in a good agreement with experiment in the region $\zeta^+ < \tilde{\zeta^+}$ and deviates from it in the region $\zeta^+ > \tilde{\zeta^+}$ (Fig.7.a and 7.b).

In Fig.8 the dependence of the average temperature T (averaged over the values of T obtained from the fitting the distributions $1/\pi \cdot dN/d\zeta^+$, dN/dp^2_T, $dN/dcos\Theta$ in the region $\zeta^+ > \tilde{\zeta^+}$) from the Table 1 on $(A_P * A_T)^{1/2}$ is presented. One can see, that T decreases linearly with the increasing of $(A_P * A_T)^{1/2}$ i.e with the increasing number of participating nucleons. This decrease of the temparature with increasing atomic number seems to be related to the fact that average multiplicity of secondaries increases with increasing atomic number, so the average energy per secondary decreases.

It is interesting to compare the temperatures extracted by means of our analysis with those extracted in the GSI experiments (FOPI, KAON and TAPS- Collaborations, see, e.g. [22,23]). The numerical values of the parameter T for pions in Au-Au collisions at 1 AGeV and our values for heaviest colliding pair are close to each other. But it should be noted that the extraction procedures are different. It seems interesting in this connection to perform the light front analysis of the GSI data.

5. CONCLUSIONS

The light front analysis of π^- – mesons from A_P (He, C, Mg, O) + A_T (Li, C, Ne, Mg, Cu, Pb) collisions has been carried out. In some region of phase space of π^- mesons ($\zeta^+ > \tilde{\zeta^+}$) the thermal equilibration seems to be reached, which is characterized by the temperature T. The variables used can serve as a possible convenient tool to study hadro-production processes in hadron-hadron, nucleus-nucleus and e^+ e^- – interactions.

A remark on the nature of maxima in $\zeta^\pm$ -distributions is in order. Recently ALEPH Collaboration observed the maxima in the ξ - distributions ($\xi = -ln\ p/p_{max}$) [24] of secondary hadrons in e^+ e^- collisions, which coincide to high precision with the predictions of perturbative QCD (see., e.g. [25,26]). The accuracy of coincidence increases when the next to leading order corrections are taken into account. So the shapes of ξ - distributions are related to the details of the underlying dynamics. Similarly, it seems that the maxima in $\zeta^\pm$ -distributions reflect the dynamics of the processes considered.

ACKNOWLEDGEMENTS

The authors express their deep gratitude to J.-P.Alard N.Amaglobeli, Sh.Esakia, D.Ferenc, A.Golokhvastov, S.Khorozov, G.Kuratashvili, J.Lukstins, J.-F.Mathiot, Z.Mente shashvili, G.Paic for interesting discussions. One of the authors (V.G.) would like to thank A.De Rujula and G.Veneziano and CERN Theory Division for the warm hospitality.

References

[1] M.Jacob and J.Tran Thanh Van Phys.Rep. C88(1982)321

[2] L.Csernai and J.Kapusta Phys.Rep. 131(1986)223

[3] H.Stöcker and W.Greiner Phys.Rep. 137(1986)277

[4] A.Abdurakhimov et al., Nucl.Phys A362(1981)376

[5] M.Anikina et al., JINR Report E1-84-785,Dubna (1984) 17

[6] M.Anikina et al., Phys.Rev. C33(1986)895

[7] N.S.Amaglobeli et al., Report N hep-ph/9703386

[8] A.A. Logunov, M.A. Mestvirishvili and Nguen van Hieu, Phys. Lett. B25 (1967) 611

[9] A.M.Baldin, Nucl.Phys. A447(1985)203

[10] P.A.M.Dirac, Rev.Mod.Phys. 21(1949)392

[11] N.Ya.Vilenkin and Ya.A.Smorodinsky Sov. J. of Exp. and Theor. Phys. JETP 47(1964)1793;
V.Garsevanishvili, V.G. Kadyshevsky, R.M.Mir-Kasimov, N.B.Skachkov Sov. J. of Theor. and Math.Phys. 7(1971)203

[12] V.Garsevanishvili, A.Kvinikhidze, V.Matveev, A.Tavkhelidze, R.Faustov Sov. J. Theor. and Math.Phys. 23(1975)310

[13] S.J.Chang, R.G.Root, T.M.Yan Phys.Rev. D7(1973)1133

[14] H.Leutwyler, Nucl.Phys. B76(1974)413

[15] A.Harindranath and J.Vary Phys.Rev. D36(1987)1141; D37(1988)1064

[16] S.J.Brodsky, H.C.Pauli In: Recent Aspects of Quantum Fields. Eds. H.Miller, H.Gausterer (Springer Verlag, Berlin, 1991)

[17] S.J.Brodsky, G.McCartor, H.C.Pauli, S.S.Pinsky. Particle World 3(1993) 109

[18] V.Garsevanishvili, Z.R.Menteshashvili. Relativistic Nuclear Physics in the Light Front Formalism (Nova Science Publishers, New York, 1993)

[19] K.G.Wilson, T.S.Walout, A.Harindranath, W.M.Zhang, R.J.Perry, St.D.Glazek Phys.Rev. D49(1994)6720

[20] B.Desplanques, V.A.Karmanov, J.F.Mathiot Nucl.Phys. A589(1995)697;
J.Carbonell, B.Desplanques, V.A.Karmanov, J.F.Mathiot. To appear in Phys. Rep.

[21] B.S.Aladashvili et al. Dubna-Kosice-Moscow-Strasbourg-Tbilisi-Warsaw Collaboration. Sov.J. Nucl.Phys. 34(1981)591;
L.S.Azhgirey et al., Phys.Lett. B387(1996)37

[22] P.Baltes et al., GSI Scientific Report 92-1, (1992) 50;
L.Venema et al., GSI Scientific Report 92-1, Darmstadt (1992) 42;
M.Pfeiffer et al., GSI Scientific Report 93-1, Darmstadt (1993) 58;
M.Appenheimer al., GSI Scientific Report 97-1,Darmstadt (1997) 58

[23] N.Herrmann Nucl.Phys. A610(1996)49c

[24] ALEPH Collaboration. CERN/PPE 96-999, to appear in Phys.Rep.

[25] C.P.Fong and B.R.Webber Phys.Lett. B229(1989)289

[26] Yu.L.Dokshitzer, V.A.Khoze, A.H.Mueller and S.I.Troyan. Basics of Perturbative QCD. (Editions Frontieres, Gif-sur-Yvette, 1991)

FIGURE CAPTIONS

Fig.1 Experimental set-up. The trigger and the trigger distances are not to scale.

Fig.2 The x_F – distribution of π^- mesons from $*$ – He(Li,C), $\triangle$ – C-Cu, $\circ$ – O-Pb interactions.

Fig.3 The $\xi^{\pm}$ – distribution of π^- mesons from $*$ – He(Li,C), $\triangle$ – C-Cu, $\circ$ – O-Pb interactions. The curve is a result of polynomial approximation of the experimental data.

Fig.4 The $\zeta^{\pm}$ – distribution of π^- mesons from $*$ – He(Li,C), $\triangle$ – C-Cu, $\circ$ – O-Pb interactions. The curves are the result of polynomial approximation.

Fig.5.a The p_T^2 distribution of π^- mesons from Mg-Mg interactions. $\circ$ – experimental data for $\zeta^+ > \tilde{\zeta^+}$ ($\tilde{\zeta^+}$=2.0), $\triangle$ – experimental data for $\zeta^+ < \tilde{\zeta^+}$. The solid line - fit of the data in the region $\zeta^+ > \tilde{\zeta^+}$ by the eq.12 using the Boltzmann distribution ; the dashed line - fit of the data in the region $\zeta^+ < \tilde{\zeta^+}$ by the eq.15.

Fig.5.b The p_T^2 distribution of π^- mesons from $*$ – He(Li,C), $\triangle$ – C-Cu, $\circ$ – O-Pb interactions for $\zeta^+ > \tilde{\zeta^+}$ ($\tilde{\zeta^+}$=2.0). The solid line - fit of the data in the region $\zeta^+ > \tilde{\zeta^+}$ by the eq.12 using the Boltzmann distribution.

Fig.5.c The p_T^2 distribution of π^- mesons from $*$ – He(Li,C), $\triangle$ – C-Cu, $\circ$ – O-Pb interactions for $\zeta^+ < \tilde{\zeta^+}$. The solid line - fit of the data in the region $\zeta^+ < \tilde{\zeta^+}$ by the eq.15.

Fig.6.a The $cos\Theta$ distribution of π^- mesons from Mg-Mg interactions. $\circ$ – experimental data for $\zeta^+ > \tilde{\zeta^+}$ ($\tilde{\zeta^+}$=2.0), $\triangle$ – experimental data for $\zeta^+ < \tilde{\zeta^+}$. The solid line - fit of the data in the region $\zeta^+ > \tilde{\zeta^+}$ by the eq.13 using the Boltzmann distribution; the dashed line - fit of the data in the region $\zeta^+ < \tilde{\zeta^+}$ by the polynomial of the 6-th degree.

Fig.6.b The $cos\Theta$ distribution of π^- mesons from $*$ – He(Li,C), $\triangle$ – C-Cu, $\circ$ – O-Pb interactions for $\zeta^+ > \tilde{\zeta^+}$. The solid line - fit of the data in the region $\zeta^+ > \tilde{\zeta^+}$ by the eq.13 using the Boltzmann distribution.

Fig.6.c The $cos\Theta$ distribution of π^- mesons from $*$ – He(Li,C), $\triangle$ – C-Cu, $\circ$ – O-Pb interactions for $\zeta^+ < \tilde{\zeta^+}$. The solid line - fit of the data in the region $\zeta^+ < \tilde{\zeta^+}$ by the polynomial of the 6-th degree.

Fig.7.a The $(1/\pi) \cdot dN/d\zeta^+$ distribution of π^- mesons from Mg-Mg interactions. $\circ$ – experimental data, the solid line – fit of the data in the region $\zeta^+ > \tilde{\zeta^+}$ by the eq.11 using the Boltzmann distribution; the dashed line – fit of the data in the region $\zeta^+ < \tilde{\zeta^+}$ by the formula $(1 - e^{-|\zeta^+|})^n$.

Fig.7.b The $(1/\pi) \cdot dN/d\zeta^+$ distribution of π^- mesons from C-Cu interactions. $\circ$ – experimental data, the solid line – fit of the data in the region $\zeta^+ > \tilde{\zeta^+}$ by the eq.11 using the Boltzmann distribution; the dashed line – fit of the data in the region $\zeta^+ < \tilde{\zeta^+}$ by the formula $(1 - e^{-|\zeta^+|})^n$.

Fig.8 The dependence of the parameter T on $(A_P * A_T)^{1/2}$ for He-Li, He(Li,C), C-Ne, Mg-Mg, C-Cu and O-Pb. The dashed line is a result of linear approximation.

TABLE CAPTIONS

Table 1. The results of the fit of the distributions of π^- – mesons in the region $\zeta^+ > \tilde{\zeta^+}$.

Table 2. The results of the fit of the distributions of π^- mesons in the region $\zeta^+ < \tilde{\zeta^+}$.

Table 1. Number of events, trigger, $\tilde{\zeta^+}$ and the results of the fit of the experimental distributions of π^- – mesons in the region $\zeta^+ > \tilde{\zeta^+}$.

$A_p - A_T$ $T(\Theta_{ch}, \Theta_n)$	$Number$ of $events$	$\tilde{\zeta^+}$	$T\ (MeV)$					
			$(1/\pi) \cdot dN/d\zeta^+$		dN/dp_T^2		$dN/dcos\Theta$	
			$Boltz$	$B-E$	$Boltz$	$B-E$	$Boltz$	$B-E$
$He - Li$ $T(0,0)$	4020	2.0	88 ± 6	88 ± 6	85 ±5	92 ±7	94 ± 12	102 ± 7
$He(Li, C)$ $T(0,0)$	6147	2.0	92 ± 5	92 ± 5	84 ± 4	90 ± 5	84 ± 9	90 ± 11
$C - Ne$ $T(2,0)$	902	2.1	82 ± 7	82 ± 7	75 ± 5	80 ± 6	90 ± 14	94 ± 19
Mg-Mg $T(2,2)$	6239	2.0	75 ± 3	75 ± 4	76 ± 2	76 ± 3	75 ± 3	78 ± 4
$C - Cu$ $T(3,3)$	1203	2.0	73 ± 3	73 ± 3	71 ± 2	74 ± 3	73 ± 6	76 ± 7
$O - Pb$ $T(2,0)$	732	2.0	55 ± 2	54 ± 1	53 ± 2	53 ± 1	54 ± 5	63 ± 4

Table 2. The results of the fit of the experimental distributions of π^- mesons in the region $\zeta^+ < \tilde{\zeta^+}$.

$A_p - A_T$	dN/dp_T^2			$1/\pi * dN/d\zeta^+$
	α	β_1 $(GeV/c)^{-2}$	β_2 $(GeV/c)^{-2}$	n
$He - Li$	0.51± 0.34	17.3 ± 1.9	7.5 ± 1.7	3.79 ± 0.20
$He(Li, C)$	0.92 ± 0.15	11.1 ± 1.6	4.5 ± 1.3	3.61 ± 0.15
$C - Ne$	0.46 ± 0.25	19.7 ± 1.8	8.4 ± 1.3	2.04 ± 0.11
$Mg - Mg$	0.85 ± 0.03	12.0 ± 0.4	4.8 ± 0.3	4.30 ± 0.06
$C - Cu$	0.86 ± 0.16	12.5 ± 2.1	4.9 ± 1.2	2.96 ± 0.11
$O - Pb$	0.71 ± 0.30	12.5 ± 2.1	8.1 ± 0.4	2.59 ± 0.10

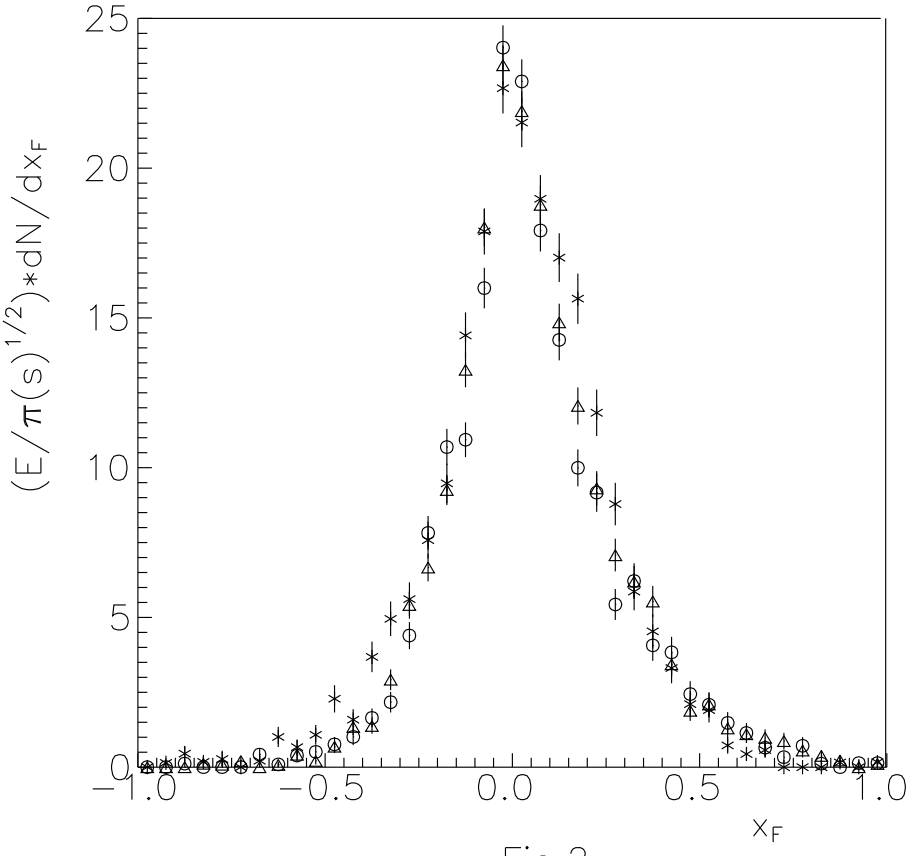

Fig.2

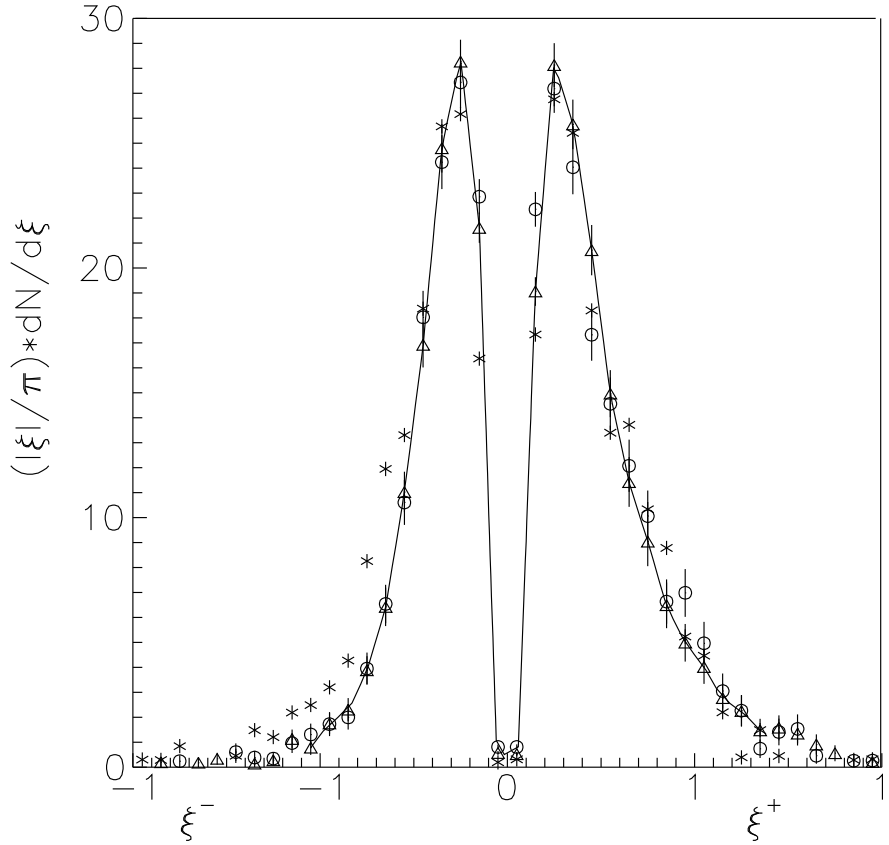

Fig.3

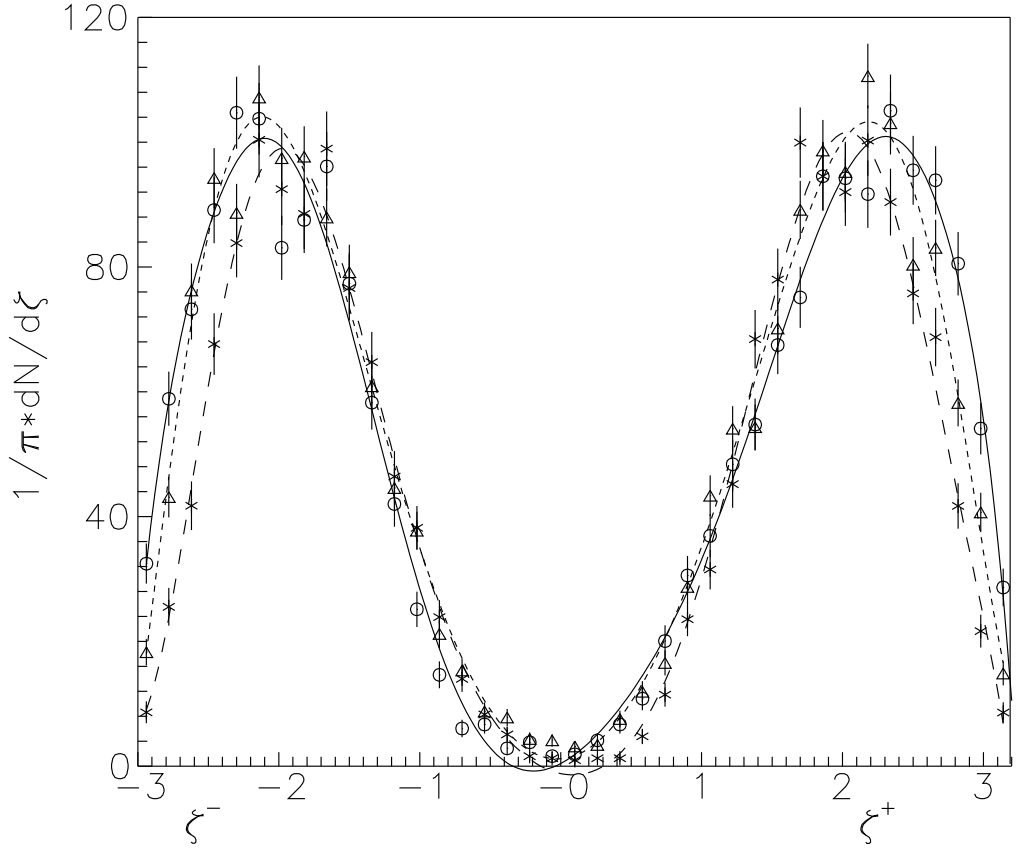

Fig.4

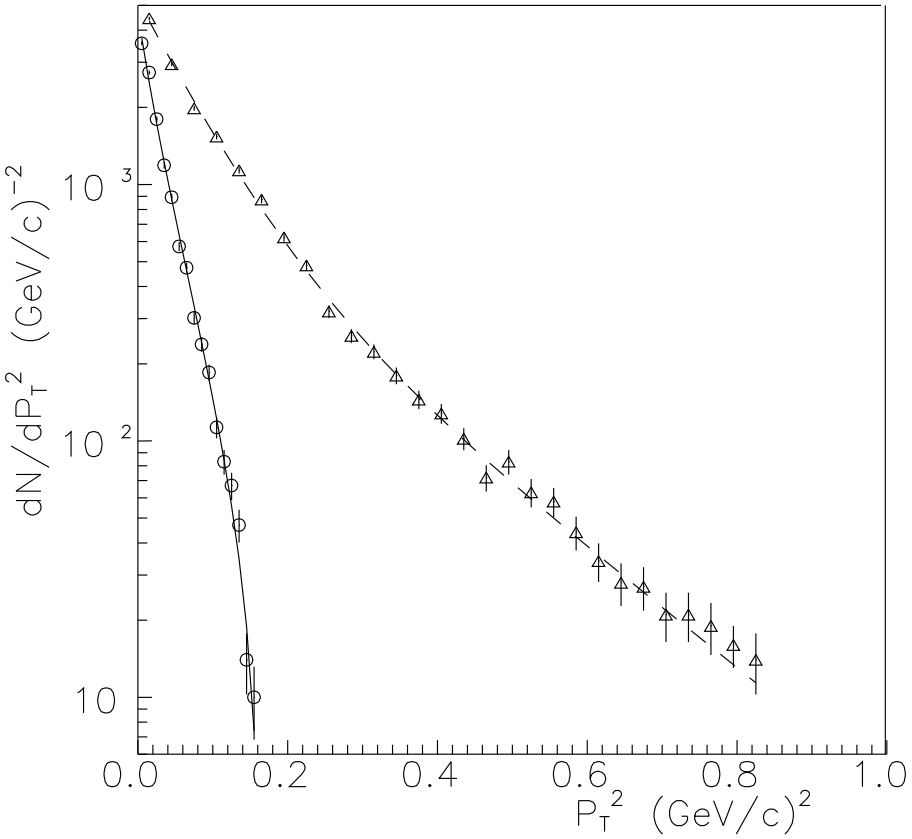

Fig.5.a

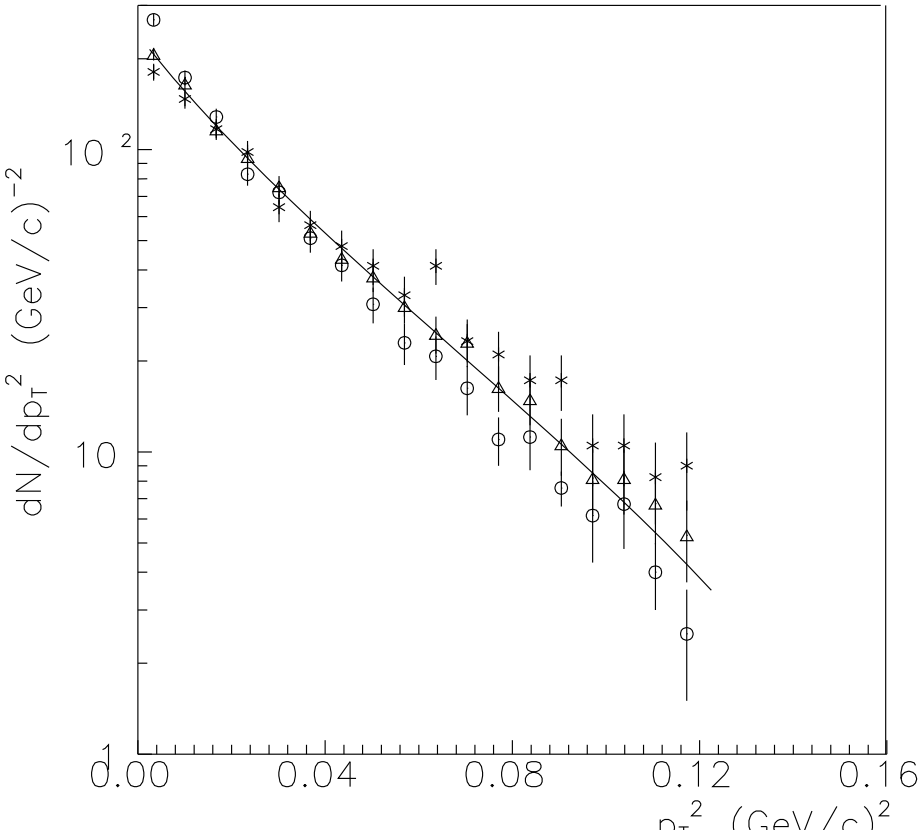

Fig.5.b

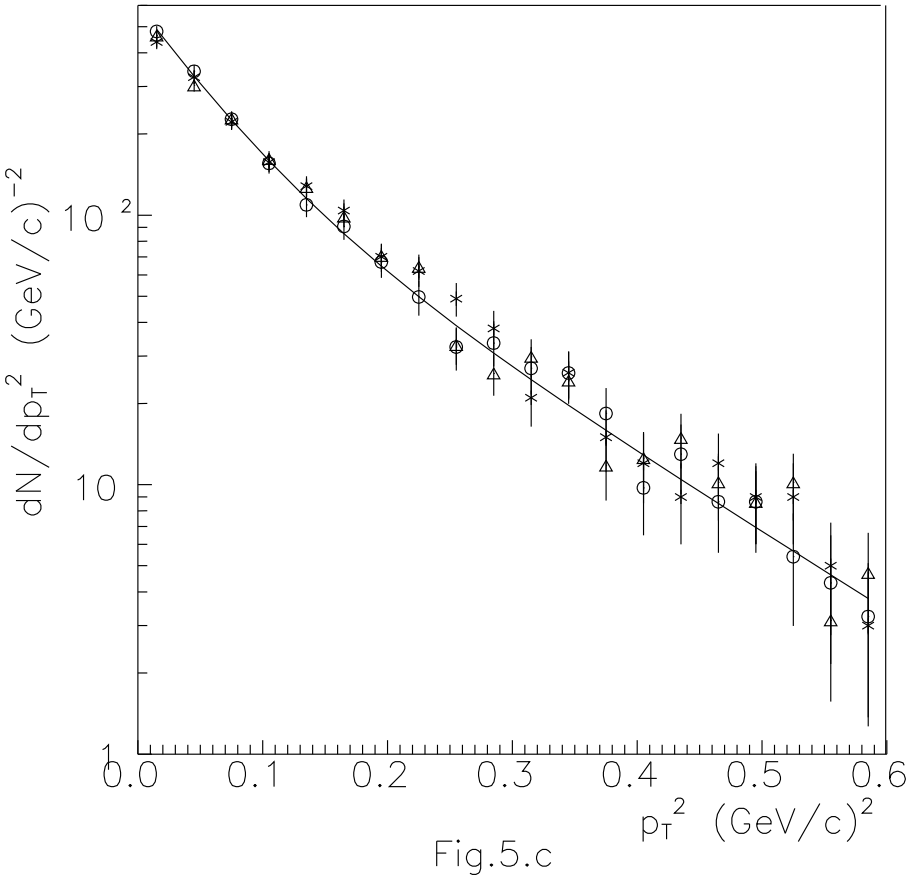

Fig.5.c

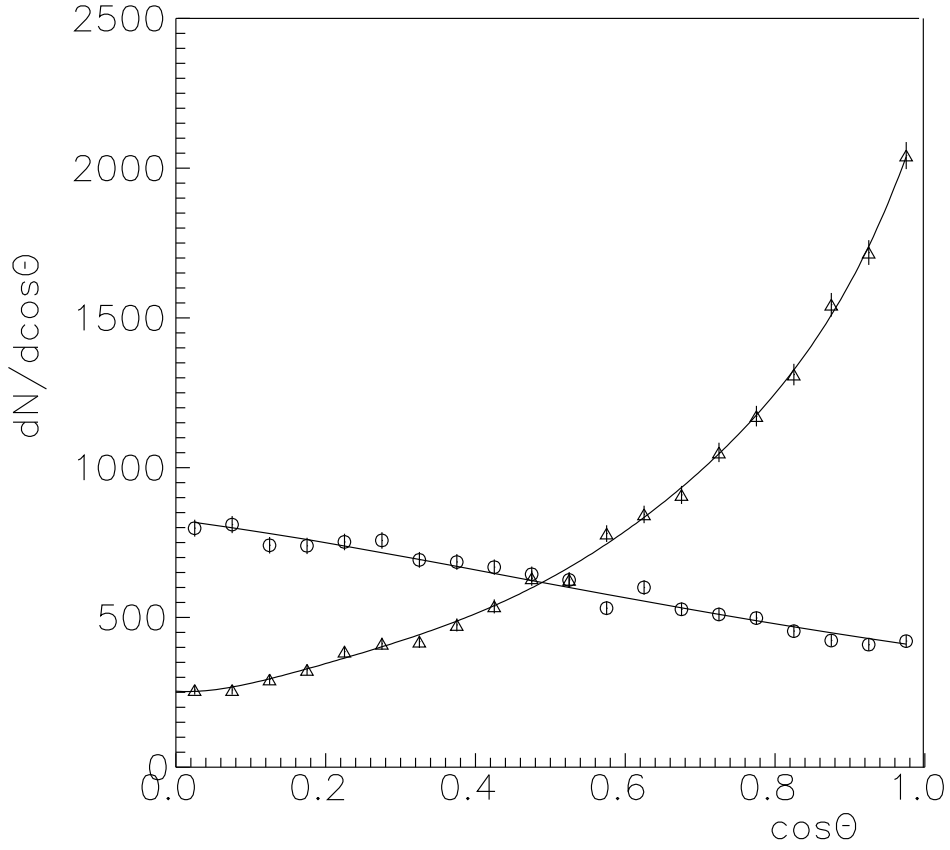

Fig.6.a

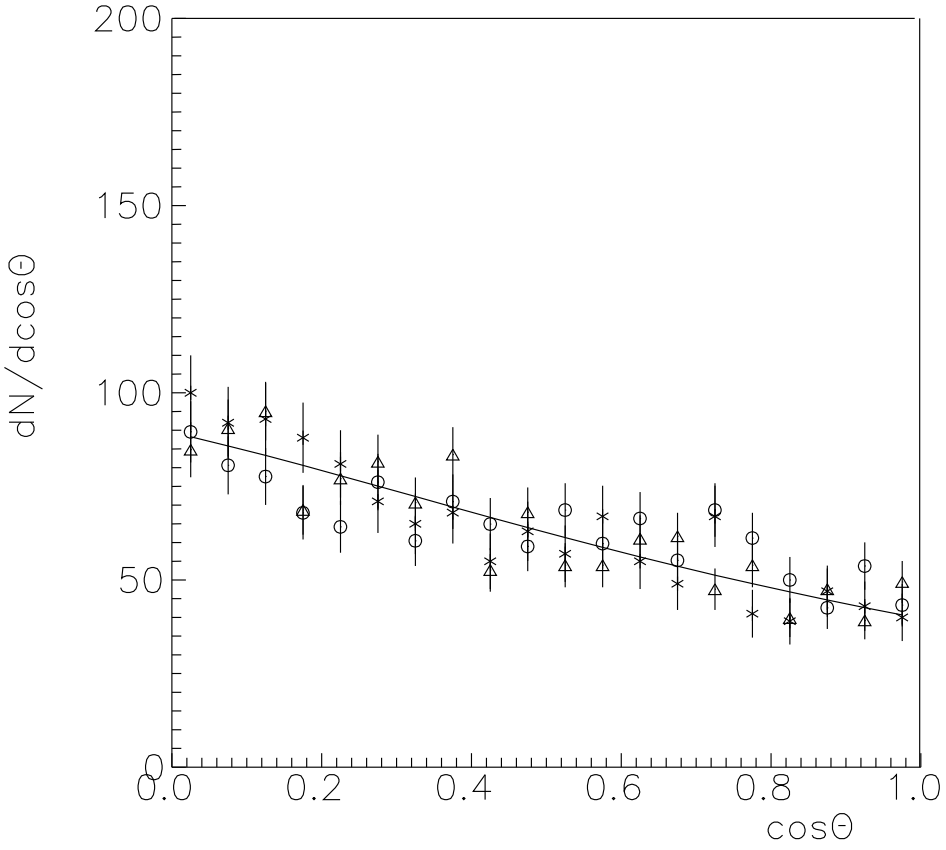

Fig.6.b

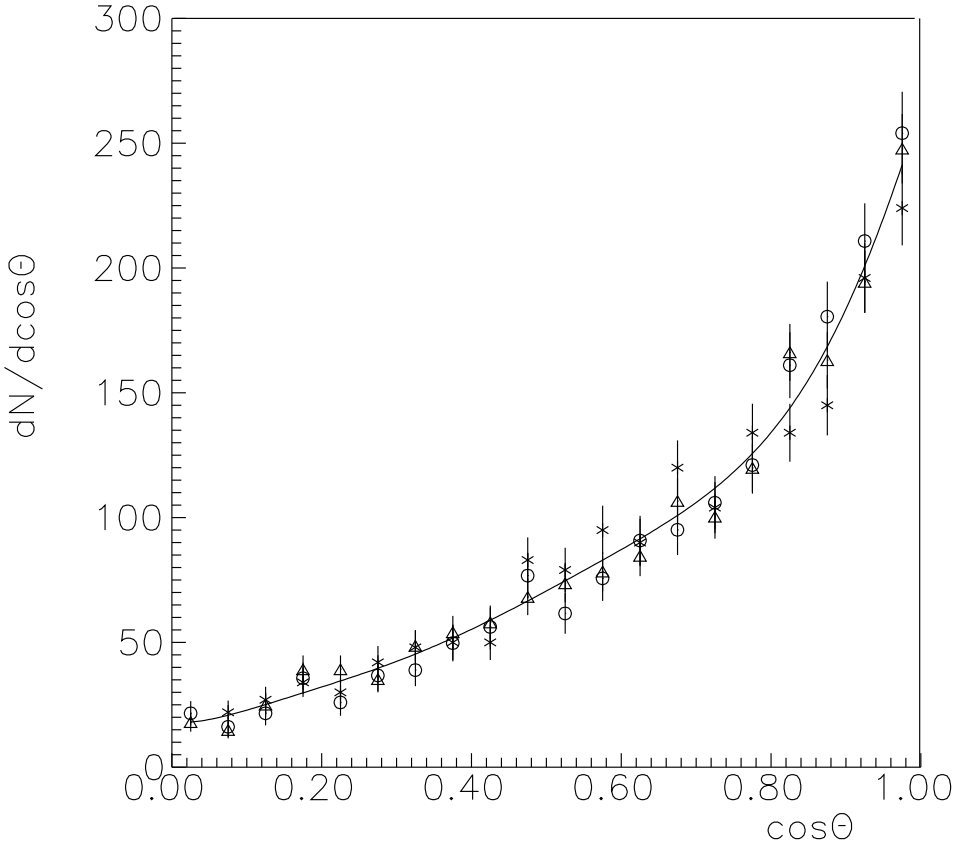

Fig.6.c

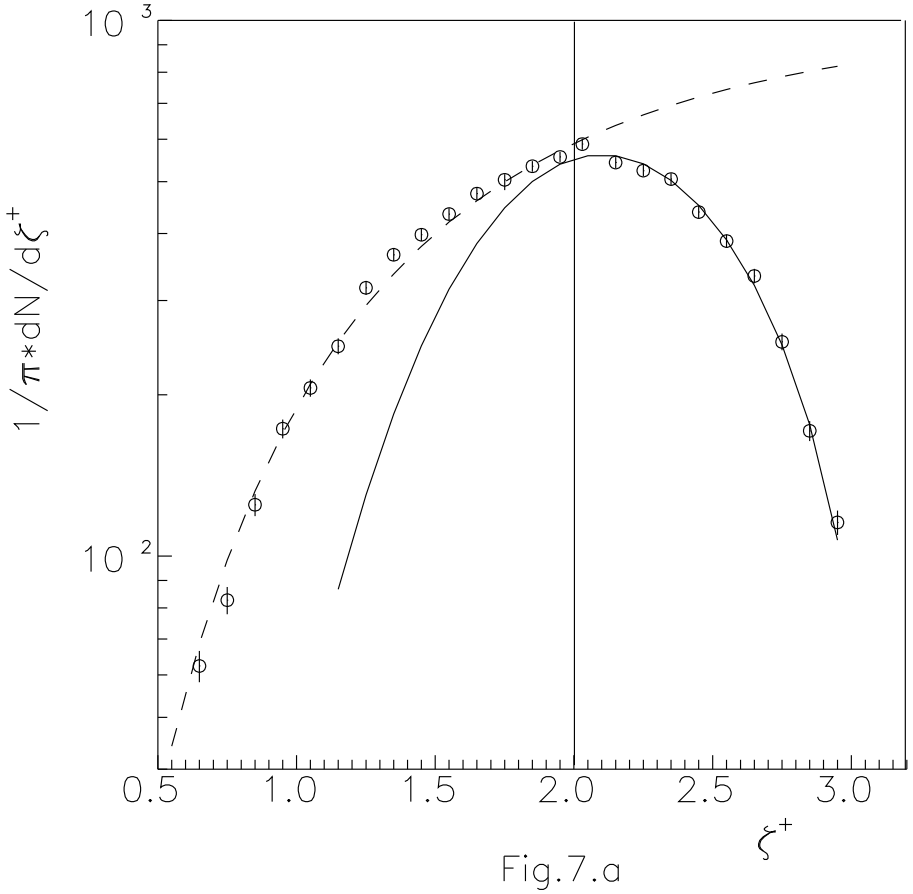

Fig.7.a

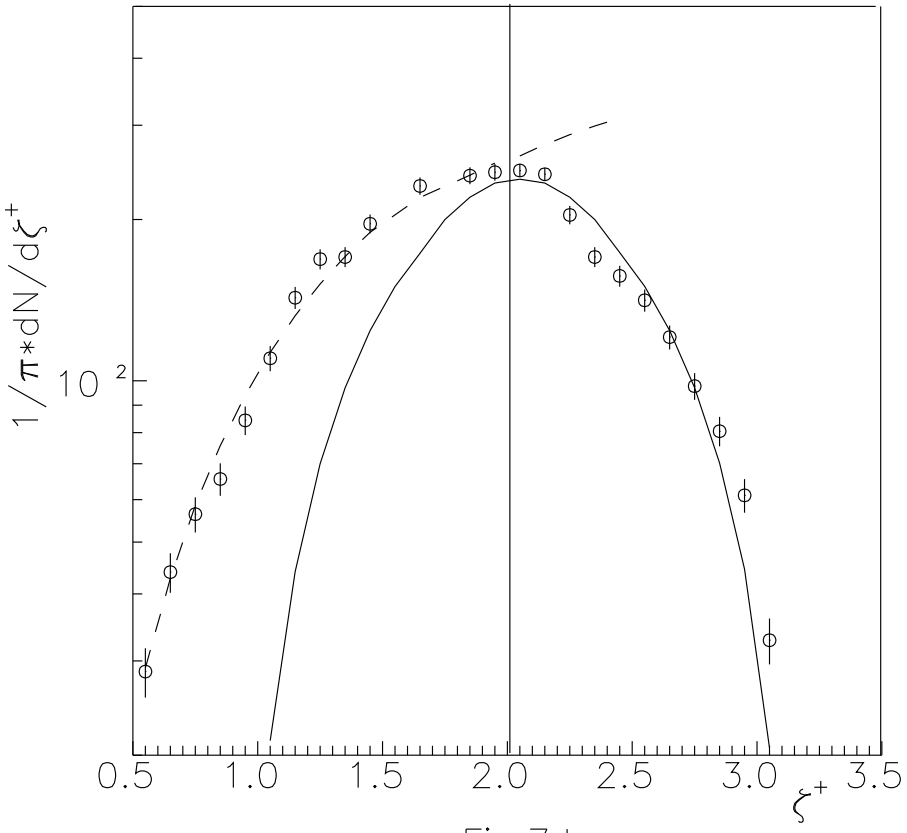

Fig.7.b

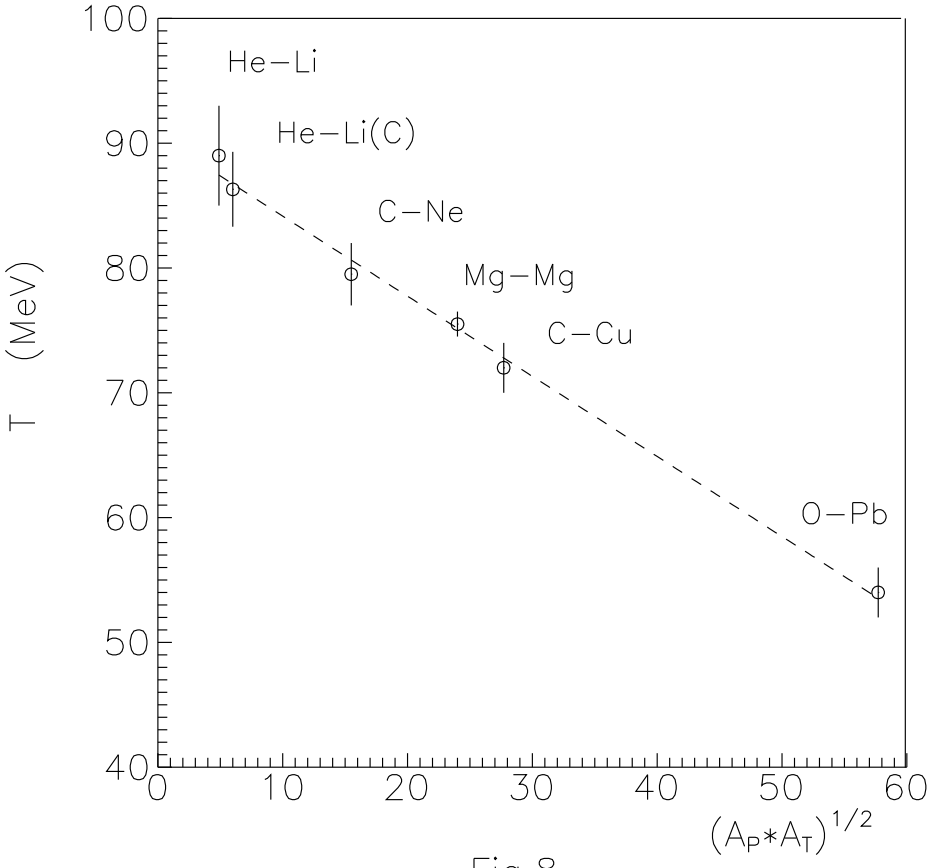
100
90
80
70
60
50
40
T (MeV)
He−Li
He−Li(C)
C−Ne
Mg−Mg
C−Cu
O−Pb
0
10
20
30
40
50
60
(A_P*A_T)^1/2

Fig.8